Quantitative Analysis of (−)-*N*-^{11}C-Propyl-Norapomorphine In Vivo Binding in Nonhuman Primates

Dah-Ren Hwang, PhD[1–3]; Rajesh Narendran, MD[1,3]; Yiyun Huang, PhD[1–3]; Mark Slifstein, PhD[1,3]; Peter S. Talbot, MD[1,3]; Yasuhiko Sudo, MD[1,3]; Bart N. Van Berckel, MD, PhD[1,3]; Lawrence S. Kegeles, MD, PhD[1,3]; Diana Martinez, MD[1,3]; and Marc Laruelle, MD[1–3]

[1]*Department of Psychiatry, Columbia University College of Physicians and Surgeons, New York, New York;* [2]*Department of Radiology, Columbia University College of Physicians and Surgeons, New York, New York; and* [3]*New York State Psychiatric Institute, New York, New York*

(−)-*N*-^{11}C-propyl-norapomorphine (^{11}C-NPA) is a new dopamine agonist PET radiotracer that holds potential for imaging the high-affinity states of dopamine D_2-like receptors in the living brain. The goal of this study was to develop and evaluate analytic strategies to derive in vivo ^{11}C-NPA binding parameters. **Methods:** Two baboons were scanned 4 times after ^{11}C-NPA injections. The metabolite-corrected arterial input functions were measured. Regional brain time–activity curves were analyzed with kinetic and graphical analyses, using the arterial time–activity curve as the input function. Data were also analyzed with the simplified reference-tissue model (SRTM) and graphical analysis with reference-region input. **Results:** ^{11}C-NPA exhibited moderately fast metabolism, with 31% ± 5% of arterial plasma concentration corresponding to the parent compound at 40 min after injection. Plasma clearance was 29 ± 1 L/h, and plasma free fraction (f_1) was 5% ± 1%. For kinetic analysis, a 1-tissue compartment model (1TCM) provided a good fit to the data and more robust derivations of the tissue distribution volumes (V_T, in mL/g) than a 2-tissue compartment model (2TCM). Using 1TCM, V_Ts in the cerebellum and striatum were 3.4 ± 0.4 and 7.5 ± 2 mL/g, respectively, which led to estimates of striatal binding potential (BP) of 4.0 ± 1.1 mL/g and striatal equilibrium specific-to-nonspecific partition coefficient (V_3'') of 1.2 ± 0.2. V_T values derived with graphical analysis were well correlated with but slightly lower than V_T values derived with kinetic analysis. V_3'' values derived with SRTM were well correlated with but slightly higher than V_3'' values derived with kinetic analysis. Using any method, a significant difference was detected in BP and V_3'' values between the 2 animals. It was determined that 30 min of scanning data were sufficient to derive V_3'' values using kinetic, graphical (arterial input and reference-region input), and SRTM analyses. **Conclusion:** This study indicates that ^{11}C-NPA is a suitable PET tracer to quantify the agonist high-affinity sites of D_2-like receptors.

Key Words: dopamine; D_2 agonist; nonhuman primate; ^{11}C-NPA; PET

J Nucl Med 2004; 45:338–346

Received Jul. 14, 2003; revision accepted Oct. 23, 2003.
For correspondence or reprints contact: Dah-Ren Hwang, PhD, New York State Psychiatric Institute, 1051 Riverside Dr., Box 31, New York, NY 10032.
E-mail: hd72@columbia.edu

The dopamine (DA) system plays an important role in the modulation of a large number of neuronal functions, including movement, drive, and reward. Alterations of DA transmissions are involved in numerous neuropsychiatric conditions, such as Parkinson's disease, schizophrenia, and substance abuse. DA receptors belong to 2 families: D_1-like (including D_1 and D_5 receptors) and D_2-like (including D_2, D_3, and D_4 receptors) (*1*,*2*). Like all G-protein–linked receptors, the affinity of D_2-like receptors for agonists is affected by the coupling of the receptors with G proteins. The high-affinity sites (D_{2high}) are G protein-coupled, whereas the low-affinity sites (D_{2low}) are those uncoupled with G protein. In vitro, approximately 50% of D_2 receptors are configured in the D_{2high} state (*3–7*).

Over the years, a large number of antagonists, such as N-^{11}C-methylspiperone and ^{11}C-raclopride, have been developed as radiotracers for imaging DA D_2-like receptors with PET. Being antagonists, these radiotracers bind with equal affinity to both the high- and the low-affinity configurations of the D_2 receptors. Therefore, these tracers do not provide information about in vivo affinity states of D_2 receptors for agonists.

The development of a D_2 receptor agonist PET radiotracer is desirable for several reasons. First, the binding of such a radiotracer would provide information about in vivo affinity of D_2 receptors for agonists in normal and disease states. Second, the in vivo binding of such a radiotracer is expected to be highly sensitive to endogenous competition and might therefore provide a superior imaging tool for probing fluctuations in endogenous DA (*8*).

Hwang et al. (*9*) recently reported a procedure to radiolabel the potent DA D_2 agonist (−)-*N*-propyl-norapomorphine (NPA) with ^{11}C, as well as on initial experiments in baboons using ^{11}C-NPA. NPA is a potent agonist at D_2 and D_3 receptors. It displays affinities of 0.27 nmol/L for D_{2high} and 26 nmol/L for D_{2low} (*3*). In baboons, ^{11}C-NPA demonstrated a rapid brain uptake with selective accumulation in the striatum, as evidenced by a striatal-to-cerebellar activi-

ties ratio of 2.86 ± 0.15 at 45 min after injection. Striatal uptake was decreased to the level of cerebellar uptake after pretreatment with the D_2 receptor antagonist haloperidol, indicating that the striatal uptake of ^{11}C-NPA was saturable and selective for D_2-like receptors. Thus, ^{11}C-NPA appeared to be a promising agonist radiotracer to label D_{2high} sites. Furthermore, experiments in rodents indicate that the in vivo binding of ^{3}H-NPA is more vulnerable to endogenous competition by DA than is ^{11}C-raclopride (*10*).

The goal of the present study was to develop and evaluate analytic strategies to derive in vivo ^{11}C-NPA binding parameters. A set of 8 PET experiments was performed on 2 baboons; both the metabolite-corrected arterial input function and the regional brain time–activity curves were measured. Data were first analyzed with compartmental kinetic analysis using the metabolite-corrected arterial time–activity curve as the input function. Both 1- (1TCM) and 2-tissue compartment models (2TCM) were evaluated. Data also were analyzed with graphical analysis, using the arterial input function. Finally, data were analyzed with graphical analysis, using a reference-region input and the simplified reference-tissue model (SRTM), both of which permit the derivation of binding parameters without measurement of arterial input function.

MATERIALS AND METHODS

Radiolabeling

The radiosynthesis of ^{11}C-NPA was performed according to our previously published procedure (*9*), with minor modifications in the purification procedure. Briefly, the crude reaction mixture was diluted with aqueous HCl and passed through a C18 Sep-Pak (Waters). The Sep-Pak was washed with diluted HCl (0.1 mol/L, 10 mL), and the tracer was recovered from the Sep-Pak using 1.5 mL ethanol. The ethanol solution was purified by semipreparative high-pressure liquid chromatography (HPLC) using an ODS-prep column (10 μm, 250 × 10 mm; Phenomenex) and a solvent mixture of 20% acetonitrile and 80% 0.1 mol/L ammonium formate with 0.5% acetic acid as previously described (*9*). The HPLC product fraction was collected, added to a diluted HCl solution (30 μmol/L, 100 mL) and passed through a C-18 Sep-Pak. The Sep-Pak was washed with 5 mL 0.1 mol/L HCl and 5 mL water. The product was recovered from Sep-Pak with ethanol (1 mL) into a sample vial containing 100 μL 3 mol/L HCl. A small portion of the solution was analyzed by analytic HPLC to determine the radiochemical purity and specific activity. The remainder of the solution was diluted with saline and filtered through a sterile 0.22 μm filter, and collected in a sterile vial.

PET Imaging Protocol

Two adult male baboons (weights: A = 30 kg, B = 20 kg) were imaged 4 times on different days with ^{11}C-NPA. Experiments were performed according to protocols approved by the Columbia–Presbyterian Medical Center Institutional Animal Care and Use Committee. Fasted animals were immobilized with ketamine (10 mg/kg intramuscularly) and anesthetized with 1.8% isoflurane through an endotracheal tube. Vital signs were monitored every 10 min, and the animals' temperatures were kept constant at 37°C with heated water blankets. An intravenous perfusion line was used for hydration and injection of radiotracers and nonradioactive drugs. A catheter was inserted in a femoral artery for arterial blood sampling. The head was positioned at the center of the field of view (FOV) as defined by imbedded laser lines. PET imaging was performed with an ECAT EXACT HR+ scanner (Siemens/CTI). In 3-dimensional mode, this camera provides an in-plane resolution of 4.3, 4.5, 5.4, and 8.0 mm in full width at half maximum at distances of 0, 1, 10, and 20 cm from the center of the FOV, respectively (*11*). A 10-min transmission scan was obtained before radiotracer injection for attenuation correction. Activity was injected intravenously over a 30-s period. Emission data were collected in 3-dimensional mode for 91 min as 21 successive frames of increasing duration (6 × 10 s and 2 × 1, 4 × 2, 2 × 5, and 7 × 10 min).

Input Function Measurements

Arterial samples were collected with an automated blood sampling system every 10 s for the first 2 min, every 20 s for the next 2 min, and manually thereafter at various intervals. A total of 29 samples was collected. After centrifugation (10 min at 1,100*g*), plasma was collected and plasma activity was measured in 0.2-mL aliquots using a γ-counter (Wallac 1480 Wizard 3M Automatic γ-counter; Perkin-Elmer).

Selected samples (n = 5 per study, collected at 1, 4, 12, 40, and 80 min after radiotracer administration) were processed by HPLC to determine the fraction of activity associated with the unmetabolized parent compound. Ascorbic acid (0.01 g/mL blood) was added to these blood samples to stabilize ^{11}C-NPA. After centrifugation, plasma (0.5 mL) was pipetted into 1 mL methanol in a small centrifuge tube. The content of the tube was mixed vigorously and centrifuged (14,000*g* for 4 min). The liquid phase was separated from the precipitates. Activity in 0.1 mL of the liquid phase was counted, and the rest was analyzed by HPLC. The HPLC eluate was fraction collected in 12 counting tubes (2.0 mL each). The HPLC system consisted of a model 510 isocratic pump (Waters), a Rheodyne injector equipped with a 2-mL sample loop (Perkin-Elmer), a C18 analytic column (ODS-prep, 10 μmol/L, 4.6 × 250 mm; Phenomenex), a Flow Cell γ-detector (Bioscan), and a Spectra/Chrom CF-1 fraction collector (Fisher Scientific). The column was eluted with a mixture of 18% acetonitrile in aqueous 0.1 mol/L ammonium formate with 0.5% acetic acid at a flow rate of 2 mL/min. Before plasma sample analysis, the retention time of the parent tracer was established by injection of a small amount of the tracer into the HPLC system.

The parent fraction was calculated as the ratio of the activity in the fractions containing the parent to the total activity collected in all the fractions. A biexponential function was fitted to the 5 measured parent fractions and used to interpolate the values between and after the measurements. The smallest exponential of the fraction of the parent curve (λ_{par}) was constrained to the difference between the λ_{cer}, the terminal rate of washout of the cerebellar activity, and the λ_{tot}, the smallest elimination rate constant of the total plasma (*12*). The input function was then calculated as the product of the total counts and the interpolated fraction parent at each time point. The measured input function values were fitted to a sum of 3 exponentials, and the fitted values were used as inputs for kinetic analyses. The clearance of the parent compound (C_L, in L/h) was calculated as the ratio of the injected dose to the area under the curve of the input function extrapolated to infinity (*13,14*). The initial plasma distribution volume (V_{bol}, in L) was

calculated as the ratio of the injected dose to peak plasma concentration.

For the determination of the plasma free fraction (the fraction of unmetabolized radioligand that is not protein bound [f_1, unitless]), 0.2-mL aliquots of plasma (collected before tracer injection and spiked with the radiotracer) in triplicates were pipetted into ultrafiltration units (Amicon Centrifree; Millipore) and centrifuged at room temperature for 20 min at 1,100*g* (*15*). The radioactivities of the plasma, the ultrafiltrate, and the filtration unit were counted, and f_1 was calculated as the ratio of the ultrafiltrate activity concentration (in μCi/μL) to the plasma activity concentration (in μCi/μL).

Image Analysis

An MR image of each baboon's brain was obtained for the purpose of identifying the regions of interest (ROIs) (T1-weighted axial MRI sequence, acquired parallel to the anterior–posterior commissure; repetition time = 34 msec; echo time = 5 msec; flip angle of 45°; slice thickness = 1.5 mm; 0 gap; matrix = 1.5 × 1.0 × 1.0 mm voxels).

Two regions were delineated on the MR image: the cerebellum (CER), a region with negligible density of D_2-like receptors, and the striatum (STR), the region with the highest density of D_2-like receptors. Previous haloperidol blocking experiments with ^{11}C-NPA failed to detect any significant displaceable ^{11}C-NPA binding in extrastriatal regions in baboons (*9*). Thus, the striatum was the only ROI analyzed.

PET emission data were attenuation corrected using the transmission scan, and frames were reconstructed using a Shepp filter (cutoff, 0.5 cycle per projection ray). Reconstructed image files were then processed using the image analysis software MEDx (Sensor Systems, Inc.). An image was created by summing all the frames, and this summed image was used to define the registration parameters for use with the MR image, using a between-modality automated image registration (AIR) algorithm (*16*). Registration parameters were then applied to the individual frames for registration to the MRI dataset. Regional boundaries were transferred to the individual registered PET frames, and the time–activity curves were measured and decay corrected. Right and left regions were averaged. For a given animal, the same regions were used for all experiments. The contribution of plasma total activity to the regional activity was calculated assuming a 5% blood volume in the ROI and subtracted from the regional activity before analysis (*17*).

Quantitative Analysis

Outcome Measures. The regional tissue distribution volume (V_T, in mL/g) was defined as the ratio of the ligand concentration in a region (C_T, in μCi/g) to the concentration of the unmetabolized ligand in the arterial plasma (C_A, in μCi/mL) at equilibrium and expressed as:

$$V_T = \frac{C_T}{C_A}. \qquad \text{Eq. 1}$$

In the cerebellum, a region with negligible D_2-like receptors, only the free and nonspecifically bound ^{11}C-NPA contributed to the V_T (i.e., in the cerebellum, V_T was equal to the nondisplaceable distribution volume of ^{11}C-NPA). In the striatum, free, nonspecifically bound and specifically bound ^{11}C-NPA contributed to the V_T. The nondisplaceable distribution volumes were assumed to be identical in the cerebellum and the striatum.

The binding potential (BP) was derived as the difference between striatal and cerebellar V_T. BP is related to receptor parameters by:

$$V_{T\,STR} - V_{T\,CER} = BP = f_1 \times \frac{B_{max}}{K_D}, \qquad \text{Eq. 2}$$

where B_{max} is the concentration of available sites (in nmol/g tissue) and K_D is the in vivo equilibrium dissociation constant of the radiotracer (in nmol/mL brain water) (*18*).

The other outcome measure of interest was the equilibrium specific-to-nonspecific partition coefficient (V_3''). V_3'' was calculated as the ratio of BP to $V_{T\,CER}$ and is related to receptor parameters by:

$$\frac{BP}{V_{T\,CER}} = V_3'' = f_2 \times \frac{B_{max}}{K_D}, \qquad \text{Eq. 3}$$

where f_2 is the free fraction in the nonspecific distribution volume of the brain ($f_2 = f_1/V_{T\,CER}$) (*18*).

Parameter Estimation. Four methods were used for parameter estimations. The first 2 methods (kinetic and graphical analysis) used the arterial time–activity curve as the input function. The third and fourth methods (SRTM and graphical analysis with reference-region input) derived the input function information from the cerebellar time–activity curve.

Kinetic Analysis. Regional V_T was derived by kinetic analysis of the regional time–activity curves using the metabolite-corrected arterial plasma concentrations as the input function, according to a 1TCM or a 2TCM. Kinetic parameters (K_1 and k_2 for 1TCM; K_1–k_4 for 2TCM) were derived by nonlinear regression using a Levenberg–Marquardt least-squares minimization procedure implemented in MATLAB (The Math Works, Inc.) as described elsewhere (*19*). In the 1TCM, K_1 (in mL/[g · min]) and k_2 (in 1/min) are the rate constants governing the transfer of the ligands in and out of the brain, respectively. In the 2TCM, K_1 and k_2 are the rate constants governing the transfer of the ligands in and out of the nondisplaceable compartment, whereas k_3 (in 1/min) and k_4 (in 1/min) describe the rate of association and dissociation to and from the receptors, respectively.

In the 1TCM, V_T was derived from kinetic parameters as:

$$V_T = \frac{K_1}{k_2}. \qquad \text{Eq. 4}$$

In the 2TCM, V_T was derived from kinetic parameters as:

$$V_T = \frac{K_1}{k_2}\left(1 + \frac{k_3}{k_4}\right). \qquad \text{Eq. 5}$$

In both cases, BP and V_3'' were derived using Equations 2 and 3. Using an unconstrained 2TCM, the Levenberg–Marquardt algorithm failed for both the striatum and cerebellum in all 8 datasets, because some kinetic parameters assumed negative values. Therefore, a constrained ($k > 0$) sequential quadratic programming algorithm (a quasi-Newton method, implemented as the function "constr.m" in MATLAB) was used. Given the unequal sampling over time (increasing frame acquisition time from the beginning to the end of the study), the least-squares minimization procedures were weighted by frame duration.

Graphical Analysis. Regional time–activity curves were graphically analyzed using the method of Logan et al. (*20*). This method allows the determination of the regional V_T of reversible ligands

without assuming a specific compartmental configuration, because the operational equation is the same whether a 1TCM or 2TCM model is assumed. BP and V_3'' were derived using Equations 2 and 3.

Simplified Reference Tissue Method (SRTM). To test the feasibility of quantification of ^{11}C-NPA V_3'' without collecting arterial plasma samples, SRTM was implemented (*21*). In this approach, the arterial input function is not explicitly measured but appears implicitly through its effect on a reference region. The estimated parameters are R_1 (equal to the ratio of K_1 in STR to K_1 in CER) and k_2 and V_3'', with the same definitions as in previous models. SRTM was implemented after vascular correction, to facilitate comparison with results from kinetic analysis using the arterial input function. R_1, k_2, and V_3'' were determined by nonlinear least-squares minimization as in kinetic methods using the arterial input functions. The least-squares fits were weighted by frame duration.

Graphical Analysis with Reference-Region Input. Regional time–activity curves were also analyzed using the reference region as input, as described by Logan et al. (*22*) to derive V_3''. This approach utilizes an implicit representation of the input function through its relationship to the reference-region time–activity curve and is the graphical analysis analog of the reference-region approach described previously.

Determination of Minimal Scanning Time

Experimental data were collected for 91 min. For all 4 methods of analysis the minimal scanning time required to achieve time-independent derivation of striatal V_3'' was evaluated by fitting the time–activity curves to shorter datasets, representing total scanning times of 81, 71, 61, 51, and 41 min. The resulting estimates of V_3'' were normalized to the V_3'' derived with the 91-min dataset. For each scan duration, the average and SD of the 8 normalized V_3'' values were calculated. Time independence was considered achieved when 2 criteria were fulfilled (*23*): the average normalized V_3'' was between 95% and 105% of the reference V_3'' (small bias), and the SD of the normalized V_3'' was $<$10% (small error). For the kinetic and graphical analyses, the minimal scanning times required to reach the time-independent derivation of V_T in the cerebellum and striatum were derived using the same criteria.

Statistical Analysis

Goodness of fit of models with different levels of complexity were compared using the Akaike Information Criterion (AIC) (*23*) and the F test (*25*). The SEs of the rate constants were given by the square roots of the diagonal of the covariance matrix C (*26*) and expressed as percentages of the parameters (coefficient of variation [%CV]). The SE of V_T was calculated as the square root of $\nabla_k V_T' C \nabla_k V_T$, where $\nabla_k V_T$ is the gradient of V_T with respect to the rate constants (*25*). Relationships between outcome measures derived with different methods were evaluated by linear regressions. The significance of differences between estimates derived by various methods was evaluated using paired *t* tests. Differences between baboons were estimated by paired *t* tests. Effects of differences in baboons' sizes were calculated as the absolute difference between the means divided by the average SDs. A 2-tailed probability of 0.05 was selected as the significance level.

RESULTS

Injected Doses

Mean ± SD and ranges of injected doses, specific activities at time of injections, and injected masses were 211 ± 74 MBq (range, 126–363 MBq), 52 ± 62 GBq/μmol (range, 8–193 GBq/mmol), and 0.13 ± 0.14 μg/kg (range, 0.01–0.43 μg/kg).

Plasma Analysis

Plasma metabolite analysis after injection of ^{11}C-NPA revealed no lipophilic metabolites. Figure 1 shows the percentage of parent compound over time. At 40 min, the parent compound contributed to 31% ± 5% of the total activity. By both AIC and F test, a sum of 3 exponentials was selected to fit the arterial parent time–activity curves (Fig. 2). Values of f_1, V_{bol}, and C_L, are provided in Table 1.

Brain Analysis

Representative V3″ images using a 1TCM with arterial input and a basis function approach (*27*) are shown in Figure 3. Activities in the cerebellum and striatum displayed early peaks (at 2 ± 1 and 8 ± 2 min, respectively), followed by a rapid washout (Fig. 4).

Kinetic Analysis. Cerebellum V_T values calculated with the 1TCM and 2TCM models are provided in Table 2. Cerebellum V_T was slightly but significantly ($P < 0.001$) larger when calculated with 1TCM than with 2TCM. The SE (%CV) of cerebellum V_T derived with 1TCM was significantly lower than that of 2TCM ($P = 0.02$; Table 2). Both 1TCM and 2TCM resulted in comparable fits to the data, with no significant difference in the AIC (paired *t* test, $P = 0.18$; Table 2). The F test for model order was not significant in any study. Therefore, the 1TCM was selected for the kinetic analysis of the cerebellum. Mean values of cerebellar K_1, k_2, and V_T derived with 1TCM for each animal are provided in Table 3. Cerebellar K_1 was significantly higher in baboon A than in baboon B ($P = 0.03$). No

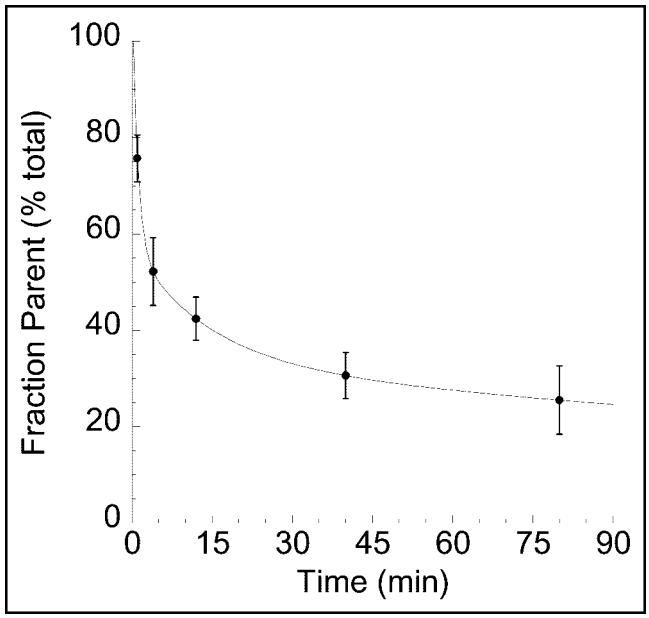

FIGURE 1. Mean ± SD fraction of plasma activity corresponding to the parent compound over time, after injection of ^{11}C-NPA in baboons ($n = 8$).

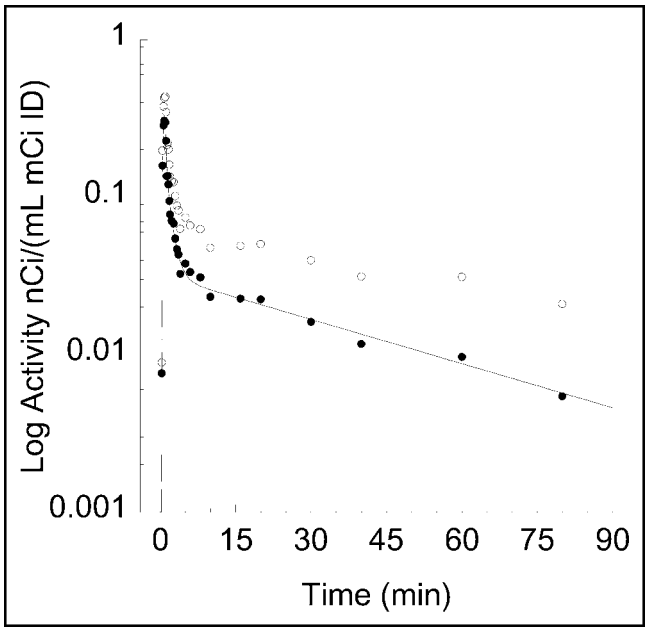

FIGURE 2. Plasma ^{11}C-NPA measurements in a typical experiment. ○ = total plasma activities; ● = activities corresponding to unmetabolized ^{11}C-NPA. Lines are values fitted to a sum of 3 exponentials.

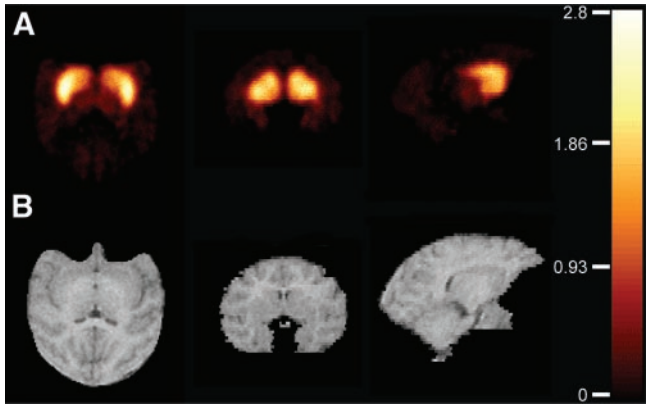

FIGURE 3. Voxelwise V_3'' map from a study (A) with coregistered MRI (B) of corresponding slices. Transaxial, coronal, and sagittal views are shown (left to right), all at the level of the striatum. These images were created by deriving VT in each voxel with kinetic analysis (1TCM) and applying Equation 3 on each voxel. Colors were scaled to V_3'' values (0–2.8). Kinetic analysis was performed using a basis function approach (*27*) in the MATLAB environment on a 1.2-GHz personal computer running the Linux operating system and completed in approximately 15 min per brain.

significant differences between baboons were observed in cerebellum V_T.

Striatal V_T values calculated with the 1TCM and 2TCM models are provided in Table 2. The striatal V_T was larger when calculated with the 1TCM than with the 2TCM ($P < 0.001$; Table 2). The SE of 1TCM striatal V_T was significantly lower than that of 2TCM striatal V_T ($P = 0.002$; Table 2). Both 1TCM and 2TCM resulted in comparable fits to the data, with no significant difference in the AIC ($P = 0.37$; Table 2). The F test was not significant in any study. Therefore, the 1TCM model was selected for the kinetic analysis of the striatum. Mean values of striatal K_1, k_2, and V_T derived with 1TCM for each animal are provided in Table 3. Striatal K_1 and V_T were significantly higher in baboon A than in baboon B ($P = 0.01$ and $P = 0.04$, respectively).

A minimal scanning time of 30 min was required to reach time invariance criteria in the derivation of V_3'' in the striatum. Figure 5 shows the small bias and error associated with progressively shorter scanning time (30–90 min). The times taken to reach time invariance criteria for the derivation of V_T in the cerebellum and striatum were 40 and 50 min, respectively.

Striatal BP and V_3'' values as derived with 1TCM are presented in Table 4. Significant ($P = 0.02$) differences between baboons were noted for both parameters (effect sizes of 1.76 and 1.86 for BP and V_3'', respectively).

Graphical Analysis with Arterial Input Function. Distribution volumes and binding parameter values derived by graphical analysis are presented in Tables 3 and 4, respectively.

TABLE 1
^{11}C-NPA Peripheral Parameters*

Baboon	f_1	V_{bol} (L)	C_L (L/h)
A	5.0% ± 0.9%	3.5 ± 0.5	30 ± 7
B	4.8% ± 0.6%	3.1 ± 0.1	29 ± 5
Average	4.9% ± 0.1%	3.3 ± 0.3	29 ± 1

*Values are mean ± SD; $n = 4$ per baboon.

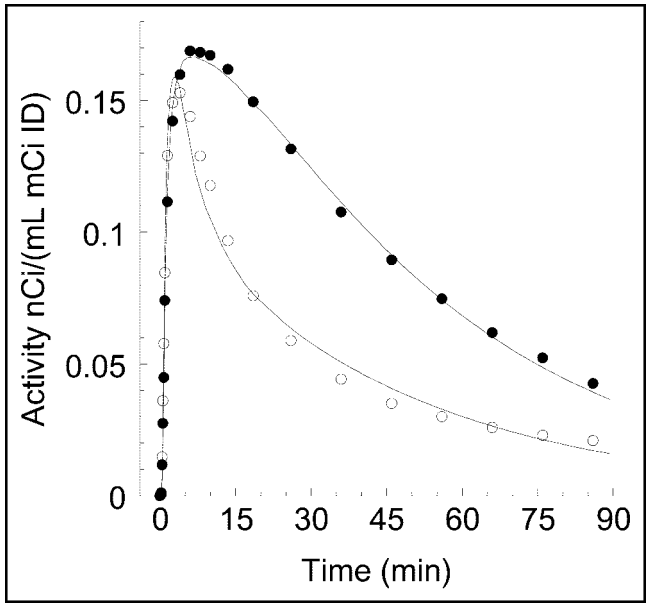

FIGURE 4. Time–activity curves in cerebellum (○) and striatum (●) after injection of ^{11}C-NPA. Points are measured values. Lines are values fitted to a 1TCM.

TABLE 2
Comparison of Compartment Models for ^{11}C-NPA Kinetic Analysis*

Region	Model	V_T (mL/g)	SE (%CV)	Goodness of fit AIC
Cerebellum	1TCM	3.4 ± 0.5	3.3 ± 1.2	−29 ± 29
	2TCM	3.3 ± 0.5†	13.6 ± 8.0†	−31 ± 32
Striatum	1TCM	7.5 ± 1.5	1.9 ± 0.8	−25 ± 38
	2TCM	7.3 ± 1.4†	4.5 ± 2.4†	−24 ± 37

*Values are mean ± SD; $n = 8$.
†Significantly different from 1TCM (paired t test; $P < 0.05$).

The time at which the regression was started (t*) was determined by visual inspection. The average t* used for analysis of the cerebellum was 42 ± 22 min and for the striatum was 62 ± 22 min. Overall, the results of graphical analysis were well correlated with kinetic analysis (Table 5). Cerebellar and striatal V_T values derived by graphical analysis were significantly lower than corresponding values derived with kinetic analysis ($P < 0.01$ for both regions). Graphical BP values were also significantly lower than kinetic BP values ($P = 0.04$). Because the graphical estimate of cerebellar V_T was lower relative to kinetic analysis (−9.4% ± 4.7%) than was the striatal V_T (−6.2% ± 3.7%), graphical V_3'' values were higher than kinetic V_3'' values ($P = 0.01$). Graphical analysis was as effective as kinetic analysis at detecting the higher site availability in baboon A compared with baboon B (with effect sizes of 1.98 and 1.93, respectively).

As observed with kinetic analysis, the minimal scanning time required to reach time invariance criteria in the derivation of striatal V_3'' (30 min) was shorter than the minimum time to reach time invariance criteria in the derivation of V_T in both the cerebellum (50 min) and striatum (60 min) with graphical analysis.

Graphical Analysis with Reference-Region Input. V_3'' values estimated with graphical analysis (Table 4) with reference-region input function were highly correlated with kinetic V_3'' values (Table 5). The average t* used for this analysis was 57 ± 11 min, determined by visual inspection. V_3'' values derived with the graphical analysis reference-region method were significantly higher than kinetic V_3'' values ($P < 0.018$). Graphical analysis V_3'' values measured in baboon A were higher than in baboon B ($P = 0.01$, effect size of 1.92). A minimal scanning time of 30 min was required to reach time invariance criteria in the derivation of striatal V_3'' with this method.

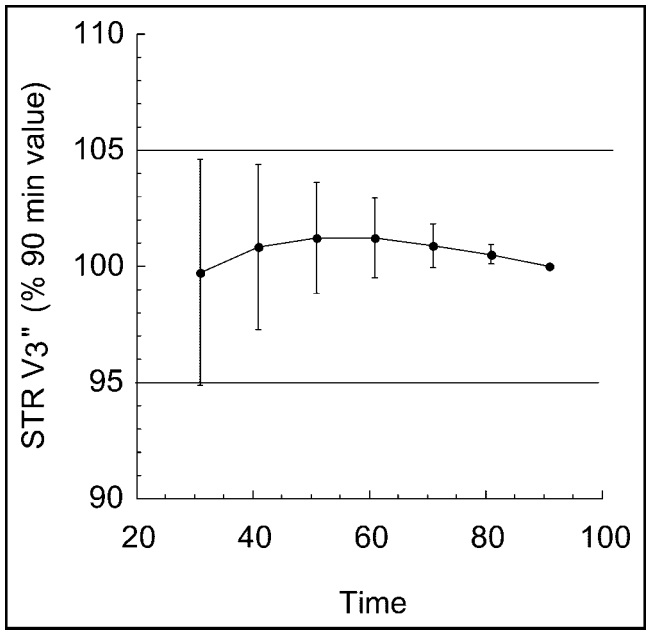

FIGURE 5. Relationship between scan duration and estimates of striatum V_3'' by kinetic analysis. For each scan duration, estimated V_3'' values were expressed in percentages of the value derived with the complete dataset (90 min). Each point is the average and SD of the 8 datasets. Decreasing the duration of scanning time from 90 to 30 min would induce only small biases and errors (<10%) on the estimates of V_3''.

SRTM Analysis. The mean value of R_1 was 0.91 ± 0.11, estimated with %CV of 4.6% ± 1.0%. SRTM V_3'' values (Table 4) were highly correlated with kinetic V_3'' values

TABLE 3
Fractional Rate Constants and Total Distribution Volumes of ^{11}C-NPA in Baboons*

	Cerebellum				Striatum			
	Kinetic analysis			Graphical analysis with arterial input	Kinetic analysis			Graphical analysis with arterial input
Baboon	K_1 (mL/g/min)	k_2 (min)	V_T (mL/g)	(V_T [mL/g])	K_1 (mL/g/min)	k_2 (min)	V_T (mL/g)	(V_T [mL/g])
A	1.06 ± 0.21	0.29 ± 0.05	3.72 ± 0.53	3.39 ± 0.45	1.11 ± 0.28	0.13 ± 0.03	8.50 ± 1.51	8.02 ± 1.40
B	0.76 ± 0.11†	0.24 ± 0.04	3.17 ± 0.31	2.90 ± 0.26	0.67 ± 0.13†	0.10 ± 0.02	6.47 ± 0.97†	6.07 ± 0.71†
Mean	0.91 ± 0.21	0.27 ± 0.03	3.44 ± 0.39	3.15 ± 0.35‡	0.89 ± 0.31	0.12 ± 0.02	7.48 ± 1.44	7.05 ± 1.38‡

*Values are mean ± SD; $n = 4$ per animal.
†Significantly different from baboon A (unpaired t test; $P < 0.05$).
‡Significantly different from values derived with kinetic analysis (paired t test; $P < 0.01$).

TABLE 4
Binding Parameters of ^{11}C-NPA in Baboons*

	BP (mL/g)		V_3'' (unitless)			
Baboon	Kinetic analysis	Graphical with arterial input	Kinetic analysis	Graphical with arterial input	Graphical with reference region input	SRTM analysis
A	4.78 ± 1.02	4.63 ± 0.98	1.29 ± 0.17	1.36 ± 0.17	1.35 ± 0.17	1.41 ± 0.18
B	3.30 ± 0.67†	3.17 ± 0.50†	1.03 ± 0.12†	1.09 ± 0.11†	1.08 ± 0.11†	1.13 ± 0.13†
Mean	4.04 ± 1.05	3.90 ± 1.03‡	1.16 ± 0.18	1.23 ± 0.19‡	1.22 ± 0.17‡	1.27 ± 0.19§

*Values are mean ± SD; $n = 4$ per animal.
†Significantly different between the 2 baboons (unpaired t test; $P < 0.05$).
‡Significantly different from values derived with kinetic analysis (paired t test; $P < 0.05$).
§Significantly different from values derived with kinetic analysis (paired t test; $P < 0.001$).

(Table 5). SRTM V_3'' values were significantly higher than kinetic V_3'' values ($P < 0.0001$). SRTM V_3'' measured in baboon A was higher than that in baboon B ($P = 0.01$, effect size = 1.77). A minimal scanning time of 30 min was required to reach time invariance criteria in the derivation of striatal V_3'' by SRTM.

DISCUSSION

The aim of this study was to develop a suitable analytic method to derive the parameters of ^{11}C-NPA in vivo binding (BP and V_3'') to agonist binding sites of the D_2 receptors. The most comprehensive strategy involved kinetic modeling based on specified compartmental configurations and using the arterial time–activity curve as input function. Three simpler approaches were also evaluated: graphical analysis (arterial input), which does not require the specification of a compartmental configuration; SRTM analysis, which makes it possible to derive V_3'' (1 of the 2 binding parameters) without measurement of the arterial input function; and graphical analysis with reference-region input, which incorporates both simplifications.

^{11}C-NPA was found to have a moderate rate of metabolism in plasma, and the percentage of parent compound at 30 min after injection was still about 30%. The mean peripheral clearance of ^{11}C-NPA was similar to that of ^{11}C-raclopride in the same 2 animals (27 ± 3 L/h) (unpublished data, 2003). The ^{11}C-NPA input function could be modeled as a sum of 3 exponentials. The plasma free fraction of ^{11}C-NPA was determined to be around 5%, which is about half that of ^{11}C-raclopride (10%) in the same baboons.

Two compartmental models were evaluated using this dataset. Given the presence of receptors in the striatum but not in the cerebellum, it was expected that a 2TCM would be required to model the striatal time–activity curve, whereas a 1TCM would be adequate for the cerebellum. In fact, the 1TCM was appropriate for both regions. In the striatum, the 2TCM converged only if the kinetic parameters were constrained to positive values, and, when it did, it was associated with a larger error in V_T than was the 1TCM. Furthermore, the 2TCM failed to improve significantly the goodness of fit compared with the 1TCM, taking into account the penalties associated with the larger number of parameters. Thus, the 1TCM emerged as an appropriate model to fit ^{11}C-NPA striatal uptake.

It has been suggested that the reliability of kinetic parameter estimation for the 2TCM model can be estimated from the impulse response fraction (IRF) (*28*). The IRF is defined as the fraction of the area under the curve attributable to the term

TABLE 5
Comparison of Outcome Measures Derived with Kinetic, Graphical, and SRTM Analysis

Comparison	Outcome	Difference	Regression equation y = mx + c	r^2
Graphical with arterial input versus kinetic	$V_{T\ CER}$	−9.4% ± 4.7%†	0.80x + 0.36	0.93
	$V_{T\ STR}$	−6.2% ± 3.7%†	0.91x + 0.20	0.97
	BP	−3.5% ± 4.2%*	0.95x + 0.04	0.97
	V_3''	−5.3% ± 4.0%*	0.98x + 0.08	0.89
Graphical with reference region input versus kinetic	V_3''	−4.5% ± 3.7%*	0.99x + 0.05	0.91
SRTM versus kinetic	V_3''	−8.5% ± 2.5%†	1.04x + 0.05	0.95

*Significantly different from values derived with kinetic analysis (paired t test; $P < 0.05$; $n = 8$).
†Significantly different from values derived with kinetic analysis (paired t test; $P < 0.001$; $n = 8$).

associated with the larger of the 2 eigenvalues of the state matrix in the 2TCM solution. Small IRFs are associated with difficulty in identifying the 2 distinct kinetic behaviors associated with 2TCM (*28*,*29*). Using the kinetic parameters from the striatal ^{11}C-NPA 2TCM model, the mean IRF for the striatum was indeed found to be small (0.8%) and similar to that for the cerebellum (0.7%). This computation supported the choice of the 1TCM. The situation in which the brain uptake in a region with significant target density is adequately modeled with a 1TCM is not infrequent. For example, a similar situation was reported for the benzodiazepine receptor antagonist ^{11}C-flumazenil (*30*) and the serotonin transporter ligands ^{11}C-McN 5652 and ^{11}C-DASB (*23*,*31*).

The value of ^{11}C-NPA V_T in the cerebellum was 3.44 ± 0.39 mL/g. This value is higher than the cerebellar V_T of ^{11}C-raclopride, measured as 0.93 ± 0.13 mL/g (n = 12; unpublished data, 2003) in the same animals. Given plasma free fractions of 5% and 10% for ^{11}C-NPA and ^{11}C-raclopride, respectively, these cerebellar V_T values indicate that the free fractions in the nondisplaceable compartment (f_2) are about 1% and 11% for ^{11}C-NPA and ^{11}C-raclopride, respectively. Thus, the nonspecific binding of ^{11}C-NPA is higher than that of ^{11}C-raclopride. Nonetheless, this value is still in the low range of nondisplaceable distribution volumes. For example, the cerebellum V_T of the serotonin transporter radiotracer ^{11}C-DASB is 17.3 ± 0.5 mL/g in baboons (n = 4) (*23*).

The striatal BP of ^{11}C-NPA was 4.04 ± 1.05 mL/g. In theory, ^{11}C-NPA BP is the sum of the BP at the high (BP_{high}) and low (BP_{low}) agonist affinity states of D_2 receptors, as expressed by expanding Equation 2 into:

$$BP = f_1(BP_{high} + BP_{low}) = f_1\left(\frac{R_{high}}{K_{D\ high}} + \frac{R_{low}}{K_{D\ low}}\right), \quad \text{Eq. 6}$$

where $K_{D\ high}$ and $K_{D\ low}$ are the affinities of ^{11}C-NPA for high- and low-affinity states, respectively, and R_{high} and R_{low} are the concentration of sites configured in high- and low-affinity states, respectively. In vitro, the affinities of ^{11}C-NPA for the high- and low-agonist–affinity sites differ by a factor of at least 50, as suggested by numerous in vitro studies (*3*,*32*–*35*). Under the assumptions that the affinity difference is 50 and that 50% of the receptors are configured in the high-affinity state, Equation 6 indicates that the contribution of BP_{low} to the total BP of ^{11}C-NPA is negligible (2%). Thus, under these assumptions, Equation 6 simplifies to:

$$BP = \frac{f_1 R_{high}}{K_{D\ high}}. \quad \text{Eq. 7}$$

Saturation experiments will be required to confirm these assumptions (i.e., to measure the in vivo values of K_{high}, K_{low}, R_{high}, and R_{low}).

The binding parameters obtained from other model-based methods (graphical and SRTM analyses) were comparable and correlated well with those obtained from kinetic analysis. Each method was equally effective at detecting the higher site availability in baboon A compared with baboon B. The observed result that V_T from graphical analysis was lower than V_T from kinetic modeling was consistent with previous studies showing a tendency of the graphical approach to underestimate V_T in the presence of statistical noise (*36*). The observation that V_3'' from SRTM was higher than that from kinetic modeling was also consistent with simulation studies showing a tendency of this method to overestimate V_3'' when the reference-region curve was well represented by 1 tissue compartment (*37*). Determination of the magnitude of these effects in humans will be required before adopting these simpler methods in clinical studies.

The striatum peak ^{11}C-NPA uptake occurred early, at 6–8 min after injection, after which a rapid washout followed. This fast kinetic of uptake is an advantage, because it permits the derivation of outcome measures with short scan duration. It was found that 50 and 60 min of data were required to derive V_T with kinetic analysis and graphical analysis, respectively. The derivation of V_3'' with all methods required only 30 min of data. Thus, ^{11}C-NPA binding parameters can be measured reliably in a relatively short scanning session, at least in baboons.

The other advantage of fast uptake kinetics is that this property will facilitate the implementation of a bolus-plus-constant-infusion protocol for ^{11}C-NPA. The bolus-plus-constant-infusion method that has been successfully developed for ^{11}C-raclopride leads to the establishment of a steady-state concentration of the parent compound in plasma and brain, which creates a state of sustained binding equilibrium at the level of the receptors (*38*,*39*). The measurement of regional radioactivities at equilibrium allows a direct determination of the distribution volumes. When applicable, the constant infusion has several advantages (*40*). For example, the scanning time can be reduced, and the parent plasma concentration can be measured using venous blood samples.

CONCLUSION

These results demonstrate that model-based methods can be used successfully in the quantification of in vivo binding of ^{11}C-NPA to D_2 receptors. Future studies need to establish the contribution of the D_{2high} and D_{2low} sites to the BP of ^{11}C-NPA as well as assess the potential of ^{11}C-NPA as an imaging tool to study fluctuations of endogenous DA concentration in vivo.

ACKNOWLEDGMENT

This work was supported in part by the National Alliance for Research on Schizophrenia and Depression Young Investigator Award from the National Institute of Mental Health (1RO1MH62089) and the Lieber Center for Schizophrenia Research at Columbia University. The authors acknowledge the superb assistance of Dr. Mohamed Ali, Dr. Osama Mawlawi, Kimchung Ngo, Jennifer Bae, Van Phan, and Rano Chatterjee.

REFERENCES

1. Seeman P, Van Tol HH. Dopamine receptor pharmacology. *Trends Pharmacol Sci.* 1994;15:264–270.
2. Vallone D, Picetti R, Borrelli E. Structure and function of dopamine receptors. *Neurosci Biobehav Rev.* 2000;24:125–132.
3. Sibley DR, De Lean A, Creese I. Anterior pituitary receptors: demonstration of interconvertible high and low affinity states of the D_2 dopamine receptor. *J Biol Chem.* 1982;257:6351–6361.
4. Seeman P, Grigoriadis D. Dopamine receptors in brain and periphery. *Neurochem Int.* 1987;10:1–25.
5. Richfield EK, Penney JB, Young AB. Anatomical and affinity state comparisons between dopamine D_1 and D_2 receptors in the rat central nervous system. *Neuroscience.* 1989;30:767–777.
6. Zahniser NR, Molinoff PB. Effect of guanine nucleotides on striatal dopamine receptors. *Nature.* 1978;275:453–455.
7. George SR, Watanabe M, Di Paolo T, Falardeau P, Labrie F, Seeman P. The functional state of the dopamine receptor in the anterior pituitary is in the high affinity form. *Endocrinology.* 1985;117:690–697.
8. Laruelle M. Imaging synaptic neurotransmission with in vivo binding competition techniques: a critical review. *J Cereb Blood Flow Metab.* 2000;20:423–451.
9. Hwang DR, Kegeles LS, Laruelle M. (−)-N-[(11)C]propyl-norapomorphine: a positron-labeled dopamine agonist for PET imaging of D(2) receptors. *Nucl Med Biol.* 2000;27:533–539.
10. Cumming P, Wong DF, Dannals RF, et al. The competition between endogenous dopamine and radioligands for specific binding to dopamine receptors. *Ann N Y Acad Sci.* 2002;965:440–450.
11. Brix G, Zaers J, Adam LE, et al. Performance evaluation of a whole-body PET scanner using the NEMA protocol. National Electrical Manufacturers Association. *J Nucl Med.* 1997;38:1614–1623.
12. Abi-Dargham A, Simpson N, Kegeles L, et al. PET studies of binding competition between endogenous dopamine and the D1 radiotracer [^{11}C]NNC 756. *Synapse.* 1999;32:93–109.
13. Rowland M, Tozer TN. *Clinical Pharmacokinetics.* 2nd ed. Philadelphia, PA: Lea & Febiger; 1989:25.
14. Abi-Dargham A, Laruelle M, Seibyl J, et al. SPECT measurement of benzodiazepine receptors in human brain with [123-I]iomazenil: kinetic and equilibrium paradigms. *J Nucl Med.* 1994;35:228–238.
15. Gandelman MS, Baldwin RM, Zoghbi SS, Zea-Ponce Y, Innis RB. Evaluation of ultrafiltration for the free fraction determination of single photon emission computerized tomography (SPECT) radiotracers: β-CIT, IBF, and iomazenil. *J Pharmaceutical Sci.* 1994;83:1014–1019.
16. Woods RP, Mazziotta JC, Cherry SR. MRI-PET registration with automated algorithm. *J Comput Assist Tomogr.* 1993;17:536–546.
17. Mintun MA, Raichle ME, Kilbourn MR, Wooten GF, Welch MJ. A quantitative model for the in vivo assessment of drug binding sites with positron emission tomography. *Ann Neurol.* 1984;15:217–227.
18. Laruelle M, Van Dyck C, Abi-Dargham A, et al. Compartmental modeling of iodine-123-iodobenzofuran binding to dopamine D_2 receptors in healthy subjects. *J Nucl Med.* 1994;35:743–754.
19. Laruelle M, Baldwin RM, Rattner Z, et al. SPECT quantification of [^{123}I]iomazenil binding to benzodiazepine receptors in nonhuman primates. I. Kinetic modeling of single bolus experiments. *J Cereb Blood Flow Metab.*1994;14:439–452.
20. Logan J, Fowler J, Volkow ND, et al. Graphical analysis of reversible radioligand binding from time–activity measurements applied to [*N*-^{11}C-methyl]-(−)-cocaine PET studies in human subjects. *J Cereb Blood Flow Metab.* 1990;10:740–747.
21. Lammertsma AA, Hume SP. Simplified reference tissue model for PET receptor studies. *Neuroimage.* 1996;4:153–158.
22. Logan J, Fowler JS, Volkow ND, Wang GJ, Ding YS, Alexoff DL. Distribution volume ratios without blood sampling from graphical analysis of PET data. *J Cereb Blood Flow Metab.* 1996;16:834–840.
23. Huang Y, Hwang DR, Narendran R, et al. Comparative evaluation in nonhuman primates of five PET radiotracers for imaging the serotonin transporters: [^{11}C]McN 5652, [^{11}C]ADAM, [^{11}C]DASB, [^{11}C]DAPA, and [^{11}C]AFM. *J Cereb Blood Flow Metab.* 2002;22:1377–1398.
24. Akaike H. A new look at the statistical model identification. *IEEE Trans Automat Contr.* 1974;AC19:716–723.
25. Landlaw EM, Distefano JJ III. Multiexponential, multicompartmental, and noncompartmental modeling. II. Data analysis and statistical considerations. *Am J Physiol.* 1984;246:R665–R677.
26. Carson RE, Parameters estimation in positron emission tomography. In: Schelbert HR, ed. *Positron Emission Tomography: Principles and Applications for the Brain and the Heart.* New York, NY: Raven Press; 1986:347–390.
27. Gunn RN, Lammertsma AA, Hume SP, Cunningham VJ. Parametric imaging of ligand-receptor binding in PET using a simplified reference region model. *Neuroimage.* 1997;6:279–287.
28. Carson RE, Kiesewetter DO, Jagoda E, Der MG, Herscovitch P, Eckelman WC. Muscarinic cholinergic receptor measurements with [^{18}F]FP-TZTP: control and competition studies. *J Cereb Blood Flow Metab.* 1998;18:1130–1142.
29. Watabe H, Channing MA, Der MG, et al. Kinetic analysis of the 5-HT2A ligand [^{11}C]MDL 100,907. *J Cereb Blood Flow Metab.* 2000;20:899–909.
30. Koeppe RA, Holthoff VA, Frey KA, Kilbourn MR, Kuhl DE. Compartmental analysis of [^{11}C]flumazenil kinetics for the estimation of ligand transport rate and receptor distribution using positron emission tomography. *J Cereb Blood Flow Metab.* 1991;11:735–744.
31. Ginovart N, Wilson AA, Meyer JH, Hussey D, Houle S. Positron emission tomography quantification of [^{11}C]-DASB binding to the human serotonin transporter: modeling strategies. *J Cereb Blood Flow Metab.* 2001;21:1342–1353.
32. Seeman P, Watanabe M, Grigoriadis D, et al. Dopamine D_2 receptor binding sites for agonists: a tetrahedral model. *Mol Pharmacol.* 1985;28:391–399.
33. George SR, Watanabe M, Seeman P. Dopamine D_2 receptors in the anterior pituitary: a single population without reciprocal antagonist/agonist states. *J Neurochem.* 1985;44:1168–1177.
34. Lahti RA, Mutin A, Cochrane EV, et al. Affinities and intrinsic activities of dopamine receptor agonists for the hD21 and hD4.4 receptors. *Eur J Pharmacol.* 1996;301:R11–R13.
35. Gardner B, Strange PG. Agonist action at D_2 (long) dopamine receptors: ligand binding and functional assays. *Br J Pharmacol.* 1998;124:978–984.
36. Slifstein M, Laruelle M. Effects of statistical noise on graphic analysis of PET neuroreceptor studies. *J Nucl Med.* 2000;41:2083–2088.
37. Slifstein M, Parsey RV, Laruelle M. Derivation of [^{11}C]WAY-100635 binding parameters with reference tissue models: effect of violations of model assumptions. *Nucl Med Biol.* 2000;27:487–492.
38. Carson RE, Breier A, Debartolomeis A, et al. Quantification of amphetamine-induced changes in [C-11]raclopride binding with continuous infusion. *J Cereb Blood Flow Metab.* 1997;17:437–447.
39. Mawlawi O, Martinez D, Slifstein M, et al. Imaging human mesolimbic dopamine transmission with positron emission tomography: I. Accuracy and precision of D_2 receptor parameter measurements in ventral striatum. *J Cereb Blood Flow Metab.* 2001;21:1034–1057.
40. Laruelle M, Abi-Dargham A, Al-Tikriti MS, et al. SPECT quantification of [^{123}I]iomazenil binding to benzodiazepine receptors in nonhuman primates. II. Equilibrium analysis of constant infusion experiments and correlation with in vitro parameters. *J Cereb Blood Flow Metab.* 1994;14:453–465.

JNM The Journal of NUCLEAR MEDICINE

Quantitative Analysis of (–)-*N*-^{11}C-Propyl-Norapomorphine In Vivo Binding in Nonhuman Primates

Dah-Ren Hwang, Rajesh Narendran, Yiyun Huang, Mark Slifstein, Peter S. Talbot, Yasuhiko Sudo, Bart N. Van Berckel, Lawrence S. Kegeles, Diana Martinez and Marc Laruelle

J Nucl Med. 2004;45:338-346.

The Journal of Nuclear Medicine is published monthly.
SNMMI | Society of Nuclear Medicine and Molecular Imaging
1850 Samuel Morse Drive, Reston, VA 20190.
(Print ISSN: 0161-5505, Online ISSN: 2159-662X)

SNMMI SOCIETY OF NUCLEAR MEDICINE AND MOLECULAR IMAGING